Simulations of turbulent flows out of spectral equilibrium using the PITM method

B. CHAOUAT[a], R. SCHIESTEL[b]

a. ONERA, bruno.chaouat@onera.fr
b. IRPHE, r.schiest@laposte.net

Résumé

La méthode de modélisation du transport par intégration partielle (PITM) qui permet de traiter continûment les régions RANS et LES sans frontière de raccordement brutale a été développée récemment pour simuler les écoulements turbulents hors équilibre spectral sur des maillages relativement lâches. Cette méthode repose sur des intégrations partielles du spectre de densité d'énergie dont la partition correspond au filtrage spectral. Celle-ci a été appliquée à une grande variété d'écoulements turbulents présentant des complexités physiques et s'est révélée prometteuse tant d'un point de vue physique que pratique. Après une présentation des principes du PITM et ses fondements dans l'espace spectral, nous aborderons différents types d'écoulements pour évaluer ses performances.

Abstract

The partially integrated transport modeling (PITM) method allowing seamless coupling between RANS and LES regions has been developed recently to perform numerical simulations of turbulent flows out of spectral equilibrium on relatively coarse grids. This method relies on partial integration over a split spectrum of the turbulent energy density, in which the given partitioning stands for spectral filtering. This method has been applied to perform a large variety of turbulent flows with specific physical complexities and proved to be a promising approach both from a physical and a practical point of view. After presenting the principle of the PITM method and its basic foundation in spectral space, we will investigate several types of flows in order to highlight its potentials.

Keywords : Turbulence modeling, PITM simulation, Out of spectral equilibrium flows.

1 Introduction

Different but complementary methods have been developed in the past fifty years for the simulation of turbulent flows [1, 2]. The direct numerical simulation (DNS) is obviously the best tool for simulating turbulent flows but is out of reach to this day even if considering supercomputers and the recent advances made in technology. Large eddy simulation (LES) has been a very useful method but still remains also extremely costly in term of computer resources at large Reynolds numbers due to the fact

that Kolmogorov scale cubed decreases rapidly according to the $R_t^{-9/4}$ power law of the turbulence Reynolds number . On the other hand, the Reynolds Averaged Navier-Stokes (RANS) method has been often used for predicting turbulent flows encountered in engineering applications with relatively low computational costs [3, 4, 5] but this one works well only for quasi-steady flows in the mean and fails to capture the large scale turbulent eddies. For these reasons, hybrid RANS/LES methods have been developed in the past decade to simulate engineering or industrial flows on coarse grids with acceptable computer resources. One can mention the main schools of modeling such as the so-called very large eddy simulation (VLES) [6], the detached eddy simulation (DES) [7, 8], the partially integrated transport modeling (PITM) method [9, 10, 11], the partially averaged Navier-Stokes (PANS) method [12, 13], the scale adaptive approach [14, 15]. Among these different methods, the PITM method gains a major interest because it bridges the RANS and LES methodologies with seamless coupling and thus avoids the overwhelming problems caused by the so-called gray zone that are usually posed by zonal hybrid RANS/LES methods. The PITM method based on the spectral theory background is identified as a continuous hybrid method that allows to perform numerical simulations of turbulent flows on relatively coarse grids when the cutoff wave number can be located before the inertial zone, as far as the grid-size is however sufficiently fine to describe correctly the mean flow, then satisfactorily results can be obtained [9, 10, 11, 16, 17, 18, 19]. As a result of interest, the PITM method reverts to DNS in the limiting condition where the grid-size in physical space Δ goes to the Kolmogorov length-scale η_K and conversely goes to RANS behavior when Δ becomes very large [10, 25, 11]. Note that PITM is a method of approach and not a mere model, because it can be used to convert almost any existing RANS model to its corresponding subfilter scale model counterpart : a second life for RANS methodology ! In particular, Schiestel and Dejoan [9] have derived two-equation subfilter scale (SFS) energy models whereas Chaouat and Schiestel [10] have developed subfilter scale stress transport models based on second-moment closure (SMC) on these bases. In this present work, after recalling the principles of the PITM method and its natural foundation in spectral space, we will investigate several types of typical flows that highlight the potentials of this PITM method. We will focus attention on turbulent flows that deserve interest in physics of turbulence from a fundamental point of view as well as engineering flows encountered in industry that are still posing major challenges in computational fluid dynamics.

2   The PITM method

2.1   Filtering process

In PITM like in LES, any turbulent variable ϕ is decomposed into a large scale (resolved part) $\bar{\phi}$ and a subfilter-scale fluctuating part $\phi^>$ (modeled part) such that $\phi = \bar{\phi} + \phi^>$. The filtered variable $\bar{\phi}$ is defined by the filtering operation as the convolution with a filter G in physical space

$$\overline{\phi} = G * \phi \tag{1}$$

that leads to the computation of a variable convolution integral

$$\bar{\phi}(\boldsymbol{x}, t) = \int_{\mathbb{R}^3} G\left[\boldsymbol{x} - \boldsymbol{\xi}, \Delta(\boldsymbol{x}, t)\right] \phi(\boldsymbol{\xi}, t) d\boldsymbol{\xi} \tag{2}$$

The instantaneous fluctuation ϕ' appearing in RANS methodology contains in fact both the large scale fluctuating part $\phi^<$ and the small scale fluctuating part $\phi^>$ such that $\phi' = \phi^< + \phi^>$. So that the ins-

tantaneous variable ϕ can then be rewritten like the sum of a mean statistical part $\langle\phi\rangle$, a large scale fluctuating part $\phi^<$ and a small scale fluctuating part $\phi^>$ as follows $\phi = \langle\phi\rangle + \phi^< + \phi^>$.

2.2 Basic equations in the spectral space

The PITM method finds its natural foundation in spectral space [23]. The theory starts with the dynamic equation of the two-point fluctuating velocity correlations in their extensions to nonhomogeneous turbulence. By using Fourier transform and performing averaging on spherical shells on the dynamic equation, one can formally derive the evolution equation of the spectral velocity correlation tensor in one-dimensional spectral space that reads [20, 21, 22]

$$\frac{\partial \varphi_{ij}(\boldsymbol{X}, \kappa)}{\partial t} + \langle u_k \rangle (\boldsymbol{X}) \frac{\partial \varphi_{ij}(\boldsymbol{X}, \kappa)}{\partial X_k} = \mathcal{P}_{ij}(\boldsymbol{X}, \kappa) + \mathcal{T}_{ij}(\boldsymbol{X}, \kappa)$$
$$+ \Psi_{ij}(\boldsymbol{X}, \kappa) + \mathcal{J}_{ij}(\boldsymbol{X}, \kappa) - \mathcal{E}_{ij}(\boldsymbol{X}, \kappa) \tag{3}$$

where in this equation, the function φ_{ij} denotes the spherical mean of the Fourier transform of the two-point velocity correlation tensor, $\mathcal{P}_{ij}$ represents the production term, $\mathcal{T}_{ij}$ is the total transfer term, Ψ_{ij} is the redistribution term, $\mathcal{J}_{ij}$ embodies all the diffusion like terms, and $\mathcal{E}_{ij}$ denotes the stress dissipation rate, $\boldsymbol{X}$ is the position midway between the two points and κ is the wave number. Exiled in one-dimensional spectral space, the turbulence quantities become only functions of the scalar wave number rather than the full wave vector. Incidentally, these spectral equations have also early been the basis for developing one-dimensional non-isotropic spectral models by the French school of turbulence [21, 23]. A full integration over the wave number space of equation (3) allows to recover formally and exactly the usual one-point statistical Reynolds stress model equations. But a partial integration over spectral slices, with a defined spectral partitioning, yields partial integrated transport equations that can be used either as the main ingredient of statistical multiple-scale models [22], or as the definition of subfilter scale turbulence used in both LES and PITM modeling [9, 10]. The PITM equations are formally obtained from integration of equation (3) in the wave number ranges $[0, \kappa_c]$, $[\kappa_c, \kappa_d]$ and $[\kappa_d, \infty[$, where κ_c is the cutoff wave number linked to the filter size Δ by $\kappa_c = \pi/\Delta$, and κ_d is the dissipative wave number located at the far end of the inertial range of the spectrum assuming that the energy pertaining to higher wave numbers is negligible [10, 11]. Then one has to identify the significant physical processes that are relevant in each spectral zone so defined. It is worthwhile to mention here that the spherical averaging operated in equation (3) implies some loss of directional information because the wave number replaces the wave vector in the parameters. One way to account for directional information is to introduce structure tensors as defined by Kassinos and Reynolds [36] that allow to distinguish dimensionality and componentality of the turbulence energy, using the terminology of these authors. The mathematical definition of the structure tensors is given in Ref. [36]. A third tensor named circulicity related to the rotational is also introduced and it is remarkable that these three tensors sum up as the turbulence kinetic energy. The work of Cambon at al. [39] developed in spectral space leads to the same type of decomposition that allows to distinguish polarization anisotropy (recalling componentality) from directional anisotropy (recalling dimensionality). More recently, a new non-linear spectral model has been developed in this line of thought by Mons et al. [37] dedicated to homogeneous anisotropic strained turbulence. A detailed account of anisotropies is thus obtained at the price of increased complexities of the model (at least 11 transport equations).

2.3 Subfilter scale eddy viscosity models

Consequently and as a result of turbulence modeling, the filtered transport equation of the subfilter scale energy reads

$$\frac{Dk_{sfs}}{Dt} = P_{sfs} - \epsilon_{sfs} + J_{sfs} \tag{4}$$

where D/Dt denotes the material derivative defined by $D/Dt = \partial/\partial t + \bar{u}_k \partial/\partial x_k$, and P_{sfs}, ϵ_{sfs} and J_{sfs} denote the production, dissipation-rate and diffusion terms, respectively. The production term P_{sfs} due to the interaction between the subfilter stress and the filtered velocity gradients is given by

$$P_{sfs} = -(\tau_{ij})_{sfs} \frac{\partial \bar{u}_j}{\partial x_i} \tag{5}$$

The turbulent stresses $(\tau_{ij})_{sfs}$ are supposed proportional to the deformation of the filtered flow field corresponding to the Boussinesq assumption

$$(\tau_{ij})_{sfs} = -2\nu_{sfs}\bar{S}_{ij} + \frac{2}{3}k_{sfs}\delta_{ij} \tag{6}$$

where S_{ij} denotes the strain deformation, the eddy viscosity is calculated from

$$\nu_{sfs} = c_\mu \frac{k_{sfs}^2}{\epsilon_{sfs}} \tag{7}$$

where c_μ is a constant coefficient. The diffusion term J_{sfs} in equation (4) is modeled by a gradient law hypothesis

$$(J_k)_{sfs} = \frac{\partial}{\partial x_j}\left[\left(\nu + \frac{\nu_{sfs}}{\sigma_k}\right)\frac{\partial k_{sfs}}{\partial x_j}\right] \tag{8}$$

where σ_k is a constant coefficient. The filtered transport equation of the subfilter dissipation rate reads

$$\frac{D\epsilon_{sfs}}{Dt} = c_{sfs\epsilon_1}\frac{\epsilon_{sfs}}{k_{sfs}}P_{sfs} - c_{sfs\epsilon_2}\frac{\epsilon_{sfs}^2}{k_{sfs}} + (J_\epsilon)_{sfs} \tag{9}$$

The diffusion term $(J_\epsilon)_{sfs}$ is also modeled using a gradient law hypothesis

$$(J_\epsilon)_{sfs} = \frac{\partial}{\partial x_j}\left[\left(\nu + \frac{\nu_{sfs}}{\sigma_\epsilon}\right)\frac{\partial \epsilon_{sfs}}{\partial x_j}\right] \tag{10}$$

where σ_ϵ is a constant coefficient. It can be shown [9, 10] that in equation (9), the coefficients in the source and sink terms can be related to their RANS counterparts by

$$c_{sfs\epsilon_1} = c_{\epsilon_1} \quad , \quad c_{\epsilon_{sfs2}} = c_{\epsilon_1} + \frac{\langle k_{sfs}\rangle}{k}(c_{\epsilon_2} - c_{\epsilon_1}) \tag{11}$$

The ratio $\langle k_{sfs}\rangle /k$ appearing in equation (11) can be calibrated as a function of the location of the cutoff wave number. To do that, we consider the universal spectrum [25]

$$E(\kappa) = \frac{\frac{2}{3}\beta(\kappa L_e)^{\alpha-1}L_e k}{[1 + \beta(\kappa L_e)^\alpha]^{\gamma+1}} \tag{12}$$

where α and β are numerical constants verifying $\alpha\gamma = 2/3$ and $\beta = (3C_K/2)^{-\gamma}$ in order to comply with the Kolmogorov law. The symbol C_K denotes the Kolmogorov constant and in practice $\alpha = 3$. Using equation (12), it is a simple matter to compute the ratio $\langle k_{sfs} \rangle /k$, leading to the expression of the coefficient $c_{\epsilon_{sfs2}}$ as

$$c_{\epsilon_{sfs2}} = c_{\epsilon_1} + \frac{c_{\epsilon_2} - c_{\epsilon_1}}{[1 + \beta\eta_c^{\alpha}]^{\gamma}} \tag{13}$$

where the parameter $\eta = \kappa L_e$ is interpreted as a dimensionless wavenumber normalized with the turbulence macroscale $L_e = k^{3/2}/\epsilon$. The function in equation (13) acting in the subfilter-scale model equation allows to sensitize the model to the grid-size Δ or in a more general way, to the filter width that is allowed to be larger than the grid-size itself [24]. The coefficient $c_{\epsilon_{sfs2}}$ can be considered as a dynamical parameter which draws the spectral distribution towards the prescribed equilibrium distribution. In other words, this term acts like a relaxation towards the Kolmogorov equilibrium spectrum.

2.4 Subfilter scale stress models

The filtered transport equation of the subfilter scale stress reads

$$\frac{D(\tau_{ij})_{sfs}}{Dt} = (P_{ij})_{sfs} + (\Pi_{ij})_{sfs} - (\epsilon_{ij})_{sfs} + (J_{ij})_{sfs} \tag{14}$$

where the terms appearing in the right-hand side of this equation are identified as the subfilter production, redistribution, diffusion and dissipation, respectively. If the frame of reference is rotating at angular velocity $\boldsymbol{\Omega}$, then the production term $(P_{ij})_{sfs}$ embodies two contributions $(P_{ij}^1)_{sfs}$ and $(P_{ij}^2)_{sfs}$. The first term accounts for the interaction between the subfilter stresses and the filtered velocity gradients and takes on the usual exact expression

$$(P_{ij}^1)_{sfs} = -(\tau_{ik})_{sfs}\frac{\partial \bar{u}_j}{\partial x_k} - (\tau_{jk})_{sfs}\frac{\partial \bar{u}_i}{\partial x_k} \tag{15}$$

The second term $(P_{ij}^2)_{sfs}$ is generated by the rotation involving the Coriolis forces

$$(P_{ij}^2)_{sfs} = -2\Omega_p\Big(\epsilon_{jpk}(\tau_{ki})_{sfs} + \epsilon_{ipk}(\tau_{kj})_{sfs}\Big) \tag{16}$$

The redistribution term $(\Pi_{ij})_{sfs}$ appearing in equation (14) is modeled assuming that the interaction mechanisms of the subgrid scales with the resolved scales of the turbulence are of the same nature than the interaction mechanisms involving all the fluctuating scales with the main flow [25]. Taking into account this argument, the redistribution term $(\Pi_{ij})_{sfs}$ is also decomposed into a slow part $(\Pi_{ij}^1)_{sfs}$ that characterizes the return to isotropy due to the action of subgrid turbulence on itself

$$(\Pi_{ij}^1)_{sfs} = -c_{1sfs}\frac{\epsilon_{sfs}}{k_{sfs}}\left((\tau_{ij})_{sfs} - \frac{1}{3}(\tau_{mm})_{sfs}\delta_{ij}\right) \tag{17}$$

and a rapid part, $(\Pi_{ij}^2)_{sfs}$ that describes the action of the filtered velocity gradients

$$(\Pi_{ij}^2)_{sfs} = -c_2\left((P_{ij}^1)_{sfs} + \frac{1}{2}(P_{ij}^2)_{sfs} - \frac{1}{3}(P_{mm}^1)_{sfs}\delta_{ij}\right) \tag{18}$$

where c_{1sfs} plays the same role as the Rotta coefficient c_1 but is no longer a true constant whereas c_2 is the same coefficient used in RANS modeling. In practice, the function c_{1sfs} is modeled as

$c_{1sfs} = c_1 \alpha(\eta)$ where α is an empirical increasing function of the parameter η to strengthen the return to isotropy for large wave numbers. The diffusion terms $(J_{ij})_{sfs}$ is modeled assuming a well-known gradient law

$$(J_{ij})_{sfs} = \frac{\partial}{\partial x_m} \left(\nu \frac{\partial (\tau_{ij})_{sfs}}{\partial x_m} + c_s \frac{k_{sfs}}{\epsilon_{sfs}} (\tau_{ml})_{sfs} \frac{\partial (\tau_{ij})_{sfs}}{\partial x_l} \right) \tag{19}$$

where c_s is a numerical constant. The subfilter tensorial transfer rate $(\epsilon_{ij})_{sfs}$ approximated by $2/3\epsilon_{sfs}\delta_{ij}$ at high Reynolds number is computed from its transport equation (9) and the diffusion term $(J_\epsilon)_{sfs}$ is then modeled by a usual tensorial gradient law

$$(J_\epsilon)_{sfs} = \frac{\partial}{\partial x_j} \left(\nu \frac{\partial \epsilon_{sfs}}{\partial x_j} + c_\epsilon \frac{k_{sfs}}{\epsilon_{sfs}} (\tau_{jm})_{sfs} \frac{\partial \epsilon_{sfs}}{\partial x_m} \right) \tag{20}$$

where c_ϵ is a numerical constant. Note that all the subfilter models described in these two latter sections have their RANS companion counterpart easily recovered when the spectral cutoff filter is put to zero. These subfilter models can also be extended to low turbulence Reynolds numbers as explained in Refs. [9, 17].

3 Illustrations to several typical turbulent flows

3.1 Decay of a turbulent flow out of spectral equilibrium

In a first example, we investigate the decay of isotropic turbulence with a perturbed spectrum departing from the standard Kolmogorov equilibrium distribution, as shown in figure 1 using the subfilter eddy viscosity turbulence model. Comparatively to the non perturbed spectrum (α), two perturbed spectra are obtained by adding a bump of energy in the large scales (β) or by a defect of energy (γ). One can see that the decay curves associated with the two perturbed spectra (β) and (γ) are both identical at the beginning of decay but afterwards they depart from the medial curve corresponding to the non-perturbed case. As a result of interest, one can observe that a peak in large scale energy (resp. a defect in large scale energy) implies a decrease (resp. an increase) of the decay rate of turbulence. These results are found
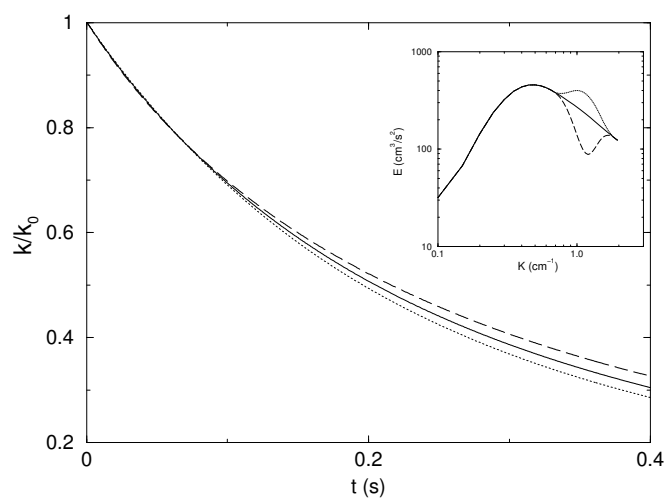

FIGURE 1 – Homogeneous decay of out of spectral equilibrium turbulence [25]. $k/k_0 = (\langle k_{sfs} \rangle + \langle k_{les} \rangle)/k_0$; $\kappa_c = 2 \, \text{cm}^{-1}$; (α) — ;(β) ... ; (γ) - - -. PITM (80^3).

to be in qualitative agreement the eddy damped quasi-normal Markovian (EDQM) spectral models

predictions obtained by Cambon [38]. These evolution can be easily explained if one considers firstly that the curves can only depart from each other after the cascade time delay required for the perturbed area to reach the dissipation zone of the three-dimensional spectrum. Then, the curves deviate from each other because the small scale energy decreases more rapidly than the large scale energy before cascading into smaller scales by non-linear interactions [25, 27]. This type of analysis involving large scales and small scales behaviors has been pointed out by Lee and Reynolds [26] in their numerical simulations of homogeneous turbulence from irrotational strains. Obviously, this spectral effect due to off equilibrium spectra cannot be reproduced using standard single scale statistical turbulence models because no spectral effect is accounted for. However models with spectral splitting including multiscale and PITM can be successful.

3.2   Mixing of turbulent flow fields of differing scales

The mixing of turbulent flows occurs in a wide variety of industrial applications or environmental situations. Generally, the mixing involves two different fields having their own levels of turbulent energy and turbulence length-scale. This situation gives rise to non-standard spectral distribution that can de-
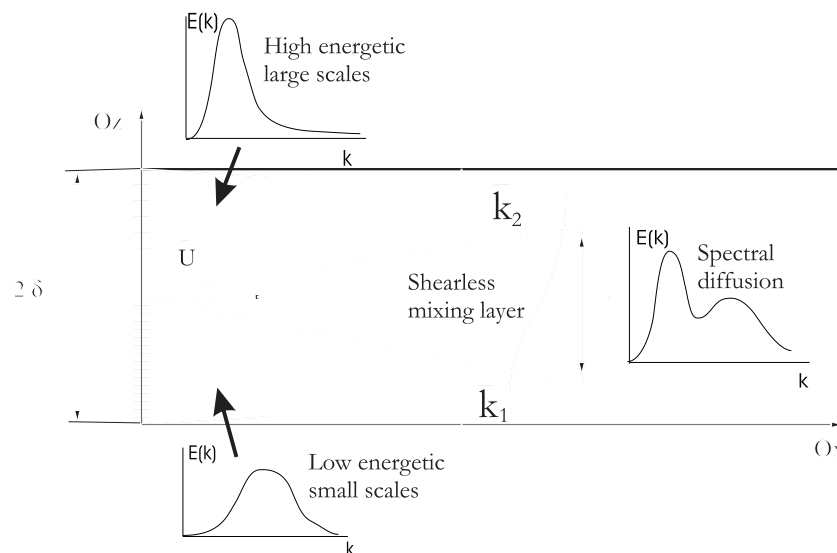

FIGURE 2 – Experimental setup of the shearless mixing layer [29] involving the mixing of turbulent fields of differing turbulence energies and scales.

part from the usual Kolmogorov distribution. The laboratory experiment of Veeravalli and Warhaft [29] investigates the typical case of a shearless mixing layer in a channel sketched in Figure 2. The spatial development of the mixing layer has been studied using the PITM approach with subfilter turbulent energy transport. Two synthetic turbulence fields are generated at the entrance of the channel with different spectral energy distributions : one loaded with large scales in the upper current and the other loaded with smaller or medium scales in the lower current (see fig. 2). The experimental setup was built using parallel bars playing the role of the generating grid, thus introducing some anisotropy at the inlet turbulence. The turbulence in the absence of shear also presents some weird behaviors, in particular the turbulent diffusion is enhanced. The numerical simulation produced the tendency to an increased diffusion in the absence of shear. This behavior has been observed in the experiment and is also in agreement with the work of Shao et al. [35] who studied the temporal mixing layer using advanced statistical spectral closures. An account of inlet anisotropy was however necessary to get energy profiles closer to the
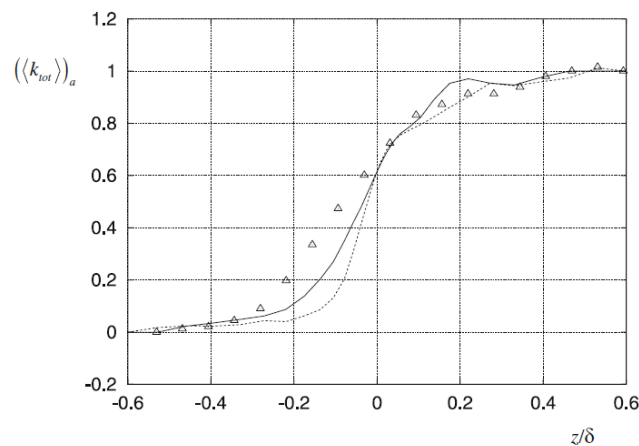
FIGURE 3 – Mixing of turbulent Flows [18]. Effect of ansisotropy of the inlet turbulence on the total turbulent energy at $x_1 = 106$ cm versus the channel height z/δ. anisotropic field, —; isotropic field, - - - -. $\triangle$, experiment [29]. PITM ($80 \times 72 \times 62$).

experimental ones (Fig. 3, note that in this figure the profiles are normalized using the maximum and the minimum values of energy). The flow is also characterized by a strong intermittent penetration of the fluid layer due to the occurrence of big eddies coming from the large scale side of the shearless mixing layer. This passage of very big eddies seems to be the reason why the turbulence energy profiles exhibit some bumps (overshoots) in the high energy side of the profiles (Fig. 3). So, the PITM method showed interesting potential for dealing with the mixing of turbulent fields having different characteristics and may be promising to tackle practical problems implying the interaction of different merging flows.

3.3　Turbulent flow subjected to spanwise rotation

Numerous applications in turbomachinery industry are concerned with flows in system rotation. These flows involve complex physical behaviors because the Coriolis forces act both directly on the mean flow and on the turbulence field. As emphasized, the Coriolis forces associated with rotation appreciably affect the mean motion and the turbulent fluctuations. In the present case, we consider a flow between
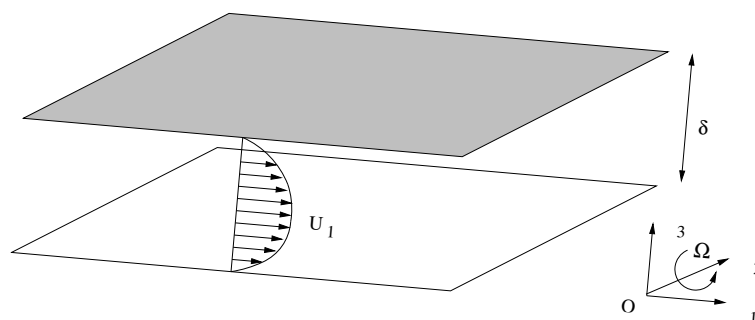

FIGURE 4 – Sketch of fully-developed turbulent channel flow in a rotating frame.

infinite parallel plates as shown by Figure 4 subjected to a spanwise rotation that is a good approximation to study internal flows within turbine blades. As the rotation rate increases, the mean flow becomes more and more asymmetric with respect to the channel centerline and the turbulence activity dramatically decreases compared to the non-rotating case, the decrease being more pronounced in the cyclonic region than in the anticyclonic wall region. The rotation is known to stabilizes the cyclonic region of
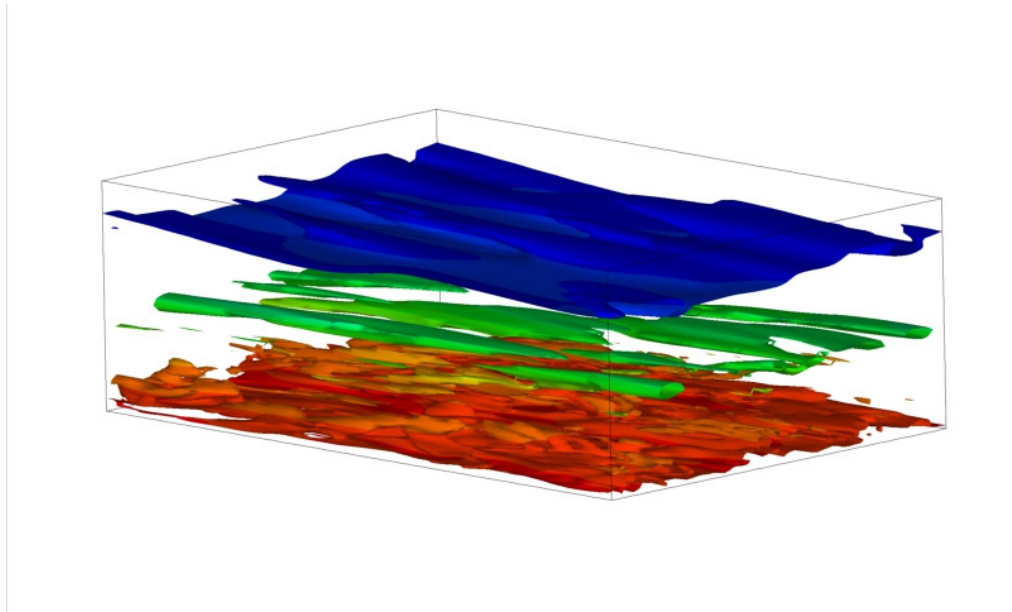
FIGURE 5 – Rotating channel flow at $Re = 14000$ and $R_o = 1.50$ [30]. Isosurfaces of vorticity modulus $\omega = 3u_m/\delta = 12.\,10^5$. Colored according to the pressure contours. Anticyclonic wall region : down ; Cyclonic wall region : up. PITM ($24 \times 48 \times 64$).

the channel flow whereas it destabilizes the anticyclonic region [31]. We have analyzed rotating flows for Reynolds number $Re = U_b\delta/\nu = 14000$ and rotations numbers $R_o = \Omega\delta/U_b = 0.17$ and 1.50 that correspond to a moderate and high rotation rate, respectively. The simulations have been performed on coarse, medium and refined grids of a channel with aspect ratio $3\delta \times 2\delta \times \delta$, but only the result associated with the coarse grid $24 \times 48 \times 64$ is here discussed for sake of conciseness of presentation. Figure 5 shows the isosurfaces of the instantaneous vorticity modulus at the high rotation rate $R_o = 1.50$. A first glimpse of sight reveals that the PITM simulation provides some dynamical elements of the flow in wall turbulence region although being performed on a coarse grid. One can see that a strong turbulence activity brought to light by the presence of very large-scale longitudinal roll cells is visible in the anticyclonic wall region. This outcome is confirmed by highly resolved LES [32]. The resolution of these structures is however relatively rough because of the coarse grid resolution. Figure 6 displays the mean dimensionless velocity profiles normalized by the bulk velocity $\langle u_1 \rangle /U_b$ as well as the turbulent shear stresses $(\tau_{13})_{sfs}/U_b^2$, $(\tau_{13})_{les}/U_b^2$, τ_{13}/U_b^2 profiles versus the global coordinates for the rotation numbers $R_o = 01.7$ and 1.5. As a result, the mean velocity presents an asymmetric character which is more and more pronounced as the rotation rate is increased. It is observed also that the velocity goes to the laminar Poiseuille solution in the cyclonic wall region at the Rotation number $R_o = 1.5$. Overall, the mean velocity profiles agree very well with the reference data [32], even if the PITM simulation is performed on a very coarse grid. The total turbulent shear stress computed as the sum of the subfilter and resolved stresses also agree relatively well with the reference data for each rotation rate [32]. At the rotation rate $R_0 = 1.5$, the shear stress goes to zero in the cyclonic region confirming that the vanishing of turbulence activity.
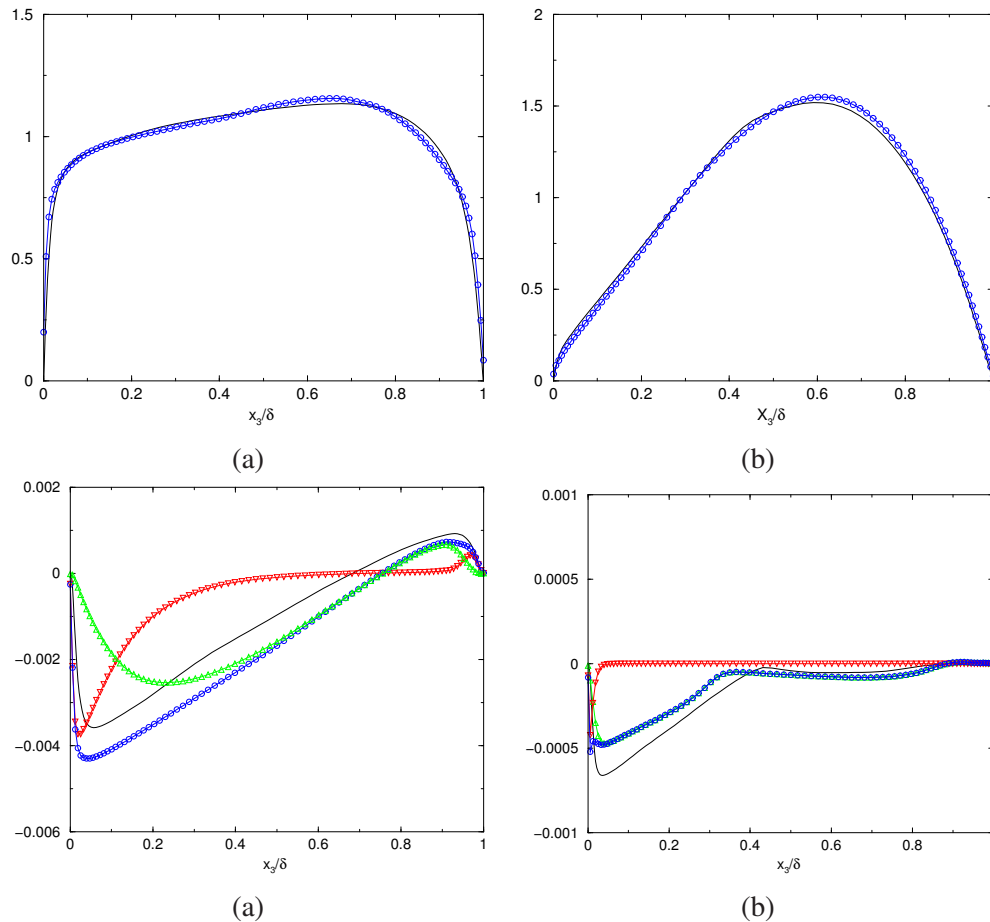
(a)

(b)

(a)

(b)

FIG. 6 – Rotating channel flow at $Re = 14000$ (a) $R_o = 0.17$; (b) $R_o = 1.50$ [30]. Mean streamwise velocity $\langle u_1 \rangle /U_b$ and turbulent shear stress τ_{13}/U_b^2 in global coordinate. $\langle u_1 \rangle /U_b$, $\circ$. $(\tau_{13})_{sfs}/U_b^2$, $\triangledown$; $(\tau_{13})_{les}/U_b^2$, $\triangle$; τ_{13}/U_b^2, $\circ$. Highly resolved LES [32], — . PITM $(24 \times 48 \times 64)$.

3.4   Turbulent flow over periodic hills at high Reynolds number

The last turbulent flow that is considered here is the channel flow over periodic hills at the high Reynolds number $Re = U_b h/\nu = 37000$ based on the hill height h and the bulk velocity U_b about the hill crest [17, 33]. This one constitutes an challenging case because of the turbulence mechanisms associated with separation, recirculation, reattachment, acceleration and wall vicinity effects that are very difficult to reproduce by numerical simulations. The PITM simulation is performed on grid of medium resolution $160 \times 60 \times 100$ accounting for approximately 1 million grid points. Figure 7 shows the streamlines plot generated in two dimensions obtained by averaging the PITM velocities both in the homogeneous planes in the spanwise direction and in time. The flow separation that is clearly visible is caused by the adverse pressure gradient resulting from the strong streamwise curvature of the lower wall. We will see in the following by investigating the velocity profile that the recirculation zone is well recovered according to the experiment [33]. Figure 8 showing the Q isosurfaces [34] of the flow reveals the presence of very large longitudinal roll cells that develop in the entire channel. Due to the flow recirculation, a strong turbulence activity is visible near the lower wall and particularly concentrated in the leeward region of the second hill. Obviously, RANS or even URANS models cannot reproduce these instantaneous roll cell structures because of their inherent long-time averaging process. Figure 9 exhibits the mean streamwise velocity $\langle u_1 \rangle /U_b$ as well as the turbulent shear stress τ_{13}/U_b^2 at two cross stations $x_1/h =$
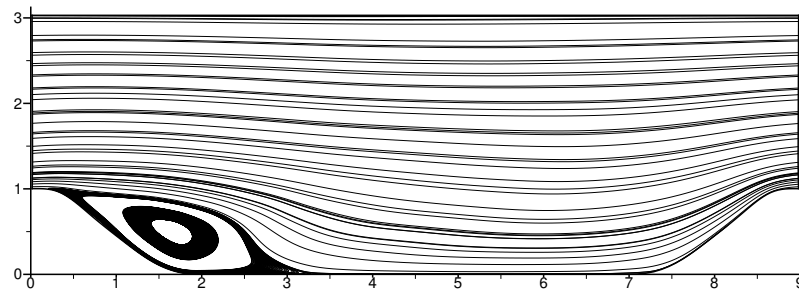
FIGURE 7 – Flow over periodic hills at $Re = 37000$ [17]. Streamlines of the average flowfield. PITM ($160 \times 60 \times 100$).
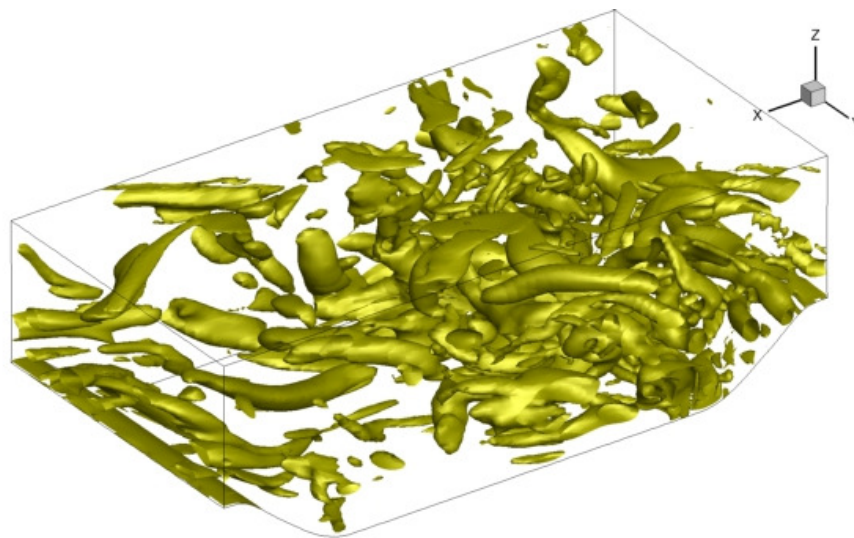

FIGURE 8 – Flow over periodic hills at $Re = 37000$ [17]. Vortical activity illustrated by the Q isosurfaces, $Q = 4\,10^5 s^{-2}$. PITM ($160 \times 60 \times 100$).

2 and 6 obtained from the PITM simulation and RSM computation, including also the experimental profiles [33]. The selected positions encompass the regions in the middle of the recirculation zone close to the leeward hill face $x_1/h \approx 2$, prior to the reattachment $x_1/h = 4$ and the flow recovery $x_1/h = 6$. At the position $x_1/h = 2$, the velocity near the wall is negative showing that the boundary layer is detached (except for the RANS-RSM calculation). The maximum reverse flow occurs in this region. But at the position $x_1/h = 6$, the boundary layer is again attached. The PITM subfilter scale stress model returns mean velocity profiles that exhibit a very good agreement with the reference data, but on the other hand, the RANS computation exhibits inaccurate results. The total shear stresses τ_{ij} includes the subfilter and resolved parts of energy. One can see that the PITM shear stress profiles present a quantitative good agreement with the reference data even if some slight differences are visible. As for the mean velocity, the RSM stresses highly deviate from the reference data in the two positions of the channel. A thorough investigation of this flow has been conducted recently [17] and has confirmed that the PITM simulation reproduces this complex flow in good agreement with the experiment [33].
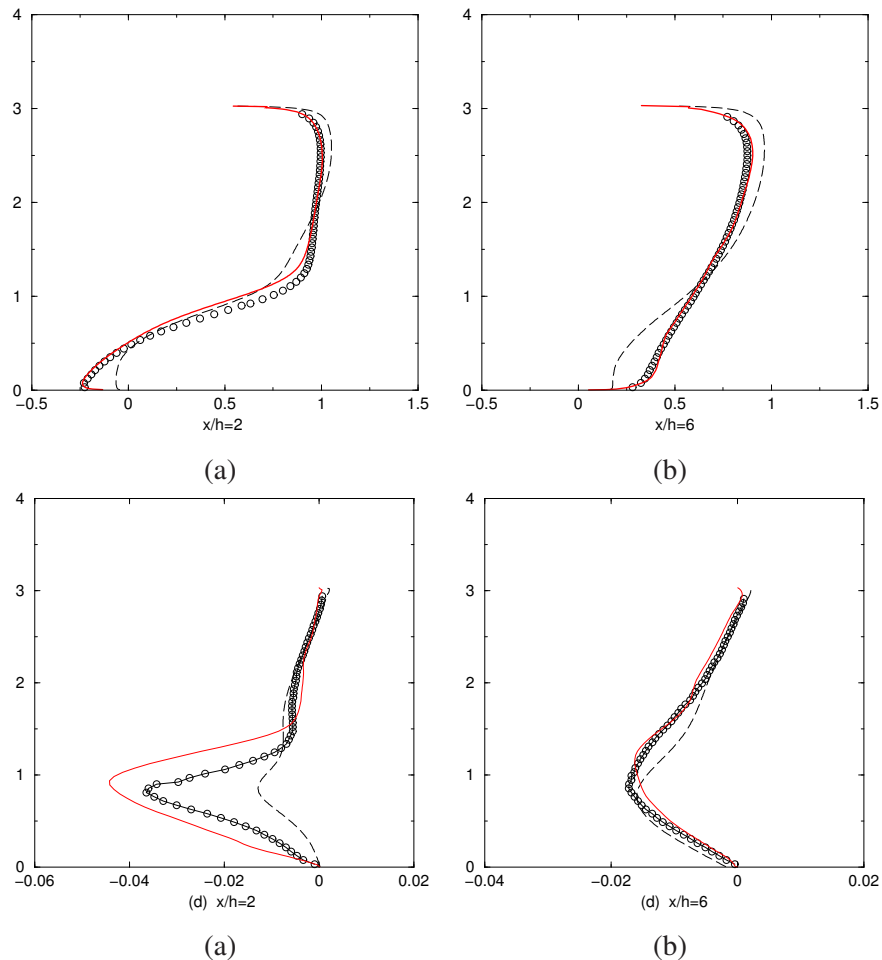
FIG. 9 – Flow over periodic hills at $Re = 37000$ [17]. Mean streamwise velocity $\langle u_1 \rangle /U_b$ and turbulent shear stress τ_{13}/U_b^2 at different locations ($x_1/h = 2$ and 6). PITM ($160 \times 60 \times 100$) —; RSM computation —($80 \times 30 \times 100$). Experiment ∘ [33].

4 A new exploration : The turbulent flow in a small axisymmetric contraction

Turbulent flow subjected to an axisymmetric contraction in the streamwise direction is encountered in many engineering applications, in the field of wind tunnels, turbomachinery, water turbines, but also in industrial processes. The effect of contraction on the mean flow is mainly to accelerate the flow while reducing the turbulence activity. But there are distortion effects on the turbulence field. Thus, the turbulent normal stress in the longitudinal direction decreases more rapidly than the two transverse stresses leading to changes in the turbulence anisotropy. In the present case, we consider grid turbulence flowing into a wind tunnel with a small axisymmetric contraction $C = 1.25$ studied in the experiment of Uberoi and Wallis [28] and sketched in Figure 10. This flow presents a complex phenomenon in physics of fluid turbulence. The anisotropy ratio of the turbulent stresses τ_{11}/τ_{22} generated by the grid is initially close to 1.4 and it then returns to unity through the contraction. But surprisingly, this ratio gradually increases again to its pre-contraction value in the uniform section downstream the contraction. This phenomenon of "return to anisotropy " constitutes a paradox which is difficult to interpret in physics of turbulence. The objective is then to investigate this complex flow by means of numerical simulations using the subfilter-scale stress model. Note that single-scale RANS models are unable to reproduce this

"return to anisotropy", contrarily to multiple-scale RANS models [22]. This simulation is very difficult to perform because of the inlet conditions. In particular, the flow details around the fine grid is extremely costly in term of computational resources, both for the number of grid-points and computer time. In the present case, the alternative solution is to create an anisotropic pseudo-random turbulence field characterized by its anisotropy ratio $\tau_{22} = \tau_{33} \approx \tau_{11}/1.4$ by means of an analytical spectral method to produce synthetic inlet conditions. As a result of the simulation performed on relatively coarse grids accounting for 2×10^6 grid-points [19], Figure 11 shows the evolution of the dimensionless bulk velocity $U_b^*(x_1) = U_b(x_1)/U_b(0)$ and the anisotropy ratio τ_{11}/τ_{22} obtained using the PITM simulation and using single-scale RSM computation. First at all, one can see that the bulk velocity passing from unity upstream the contraction to 1.25 downstream the contraction agrees perfectly well with the experimental data. As expected, the anisotropy ratio τ_{11}/τ_{22} initially close to 1.4 in the entrance of the channel gradually decreases to unity in the contraction zone suggesting that the turbulence goes to an apparent isotropic state. But as a result of simulation, it is found that this ratio increases again in the straight section downstream the contraction according to the experiment. To understand the origin of this reappearance of anisotropy, Uberoi and Wallis have advanced some qualitative arguments based on the turbulence scales relaxation. A plausible explanation is that the turbulence state just after the contraction is just an appearance in which the anisotropy of the small scales exactly compensates the anisotropy of the large scales. After the contraction, the small scales do relax rapidly, while the large scale anisotropy is more permanent and thus relaxes only slowly. The overall anisotropy can then reappear in the downstream straight section of the channel. Schiestel [27] has performed an LES simulation of decaying turbulence in a cubic box with an initial energy spectrum perturbed by introduction of anisotropy in Fourier modes. Physically, this simulation corresponds to the evolution of the flow from an initial state of turbulence that is similar to the one of the wind tunnel of Uberoi and Wallis [28] just downstream the contraction zone with a compensation between small and large scales anisotropies such that $\tau_{11}/\tau_{22} = 1$. As a result shown in Figure 3 of Ref. [27], Schiestel also observed an increase of anisotropy downstream, highlighting the scale relaxation effect described above. In the present case, this analysis is confirmed point to point by the data obtained from the PITM simulation as indicated in Table 1 showing a compensating effect between the small scales and the large scales.
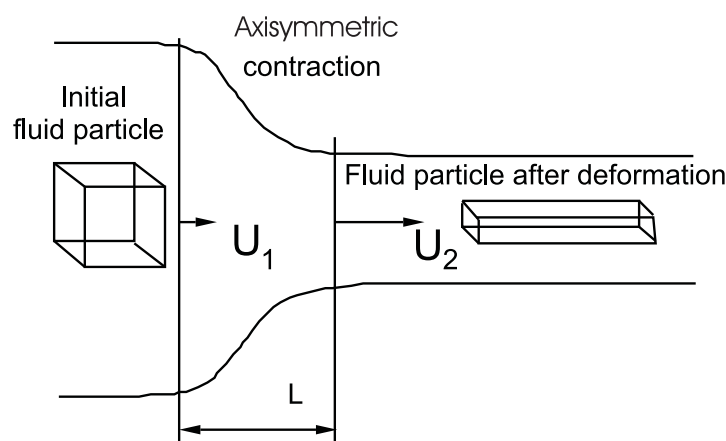

FIGURE 10 – View of axisymmetric contraction.

The new non-linear spectral model by Mons et al. [37] considers, among others, the application to homogeneous turbulence subjected to axisymmetric expansion or contraction. They suggest that the difference in the relaxation rates between directional anisotropy and polarization anisotropy included
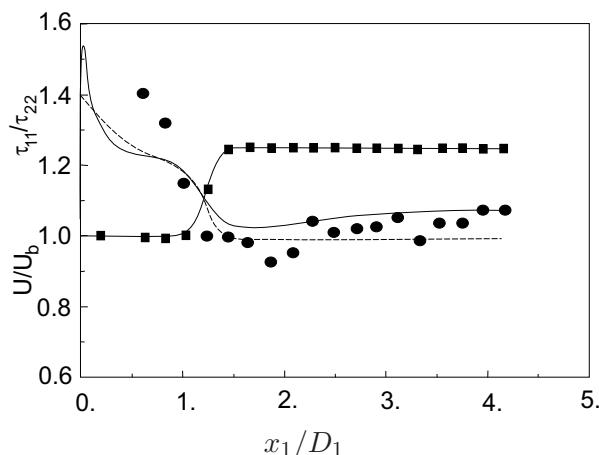
FIGURE 11 – Flow in a small axisymmetric contraction at $Re = 4.47 \times 10^5$ [19]. Evolution of the dimensionless bulk velocity $U_b^*(x_1)$, and the ratio τ_{11}/τ_{22} on the centerline of the channel in the streamwise direction. Bulk velocity $U_b^*(x_1)$: ■, experiment [28] ; —, PITM. Energy ratio τ_{11}/τ_{22} : ●, experiment [28] ; —, PITM ; – – –, Single scale RSM model. PITM ($200 \times 100 \times 100$).

x_1/D_1	$(\tau_{11})_{sfs}$	$(\tau_{22})_{sfs}$	$(\tau_{11})_{les}$	$(\tau_{22})_{les}$	τ_{11}	τ_{22}
0	0.204	0.146	0.246	0.178	0.451	0.324
1	0.0456	0.0457	0.0368	0.0246	0.082	0.070
1.5	0.0299	0.0338	0.0252	0.0206	0.0551	0.0542
4.	0.0128	0.0129	0.0074	0.0057	0.0202	0.0187

$\tau_{ii} = (\tau_{ii})_{sfs} + (\tau_{ii})_{les}$

TABLE 1 – Flow in a small axisymmetric contraction. Turbulent stresses ($\mathrm{m^2/s^2}$) at different locations in the centerline of the channel.

in their model, allows to interpret the apparent delay in the evolution of total anisotropy in these cases. Kassinos and Reynolds [36] have also analyzed this behavior and suggested that the cause may be related to the relaxation rate of the circulicity tensor which appears to be much smaller than for the dimensionality tensor. Circulicity seems like insensitive to strain rate. The explanation advanced in the present paper like in Schiestel [27] and based on cancelation between small scale anisotropy and large scale anisotropy in the energetic sense shows that directional properties are not absolutely necessary to explain this seemingly anomalous behavior. Further insights would be necessary to get a more detailed analysis, but it is not impossible that both explanations are indeed effective ? Note however, that in the present calculation the resolved eddies being part of the large eddy simulation they do include directional effects, but of course this is not the case in the subfilter model.

5   Concluding remarks and perspectives

We have recalled the basic principles of the partially integrated transport modeling method which has been especially developed for the simulation of turbulent flows on coarse grids. The method allows a huge reduction of the computational resource in comparison with the one required for highly resolved simulation. Indeed, considering that advanced closures have been used to model the subfilter range, then, large filter widths can be used without prejudice. This method has been applied to the simulation of a large variety of turbulent flows ranging from laboratory flows to engineering flows. In particular,

the PITM method has fairly well reproduced turbulent flows out of spectral equilibrium both in the energetic sense and spectral anisotropy sense, such as the flow accounting for a perturbed spectrum of energy, the mixing of turbulent flows including different levels of turbulence energy and different scales, the flow subjected to a spanwise rotation leading to cyclonic and anticyclonic wall regions, and also, the flow over periodic hills with detachment and reattachment of the boundary layer. More recently, the new exploration of the flow in a small axisymmetric contraction involving an apparently anomalous isotropy state of turbulence and the "return to anisotropy ", has been performed and a discussion of possible physical explanations of the anisotropy behavior has been advanced. Because of its potentials, more generally speaking, the PITM method is more and more used in the field of turbulence modeling for simulating complex flows from a practical point of view by users involved in CFD. Moreover, its rational formalism developed in the spectral space allowing to bridge the RANS and LES methodologies from a theoretical point of view opens the route to new perspectives in term of turbulence modeling.

Références

[1] R. Schiestel, *Modeling and simulation of turbulent flows*, ISTE Ltd and J. Wiley, 2008.

[2] K. Hanjalic, B.E. Launder, *Modelling turbulence in engineering and the environment. Second-moment route to closure*, Cambridge University Press, 2011.

[3] B. Chaouat, Numerical prediction of channel flows with fluid injection using a Reynolds stress model, Journal Propulsion and Power. **18**, (2002) 295-303.

[4] B. Chaouat, R. Schiestel, "Reynolds stress transport modelling for steady and unsteady channel flows with wall injection, Journal of Turbulence, **3**, (2002), 1-15.

[5] B. Chaouat, Reynolds stress transport modeling for high-lift airfoil flows, AIAA Journal, **44**, (2006) 2390-2403.

[6] C.G. Speziale, Turbulence modeling for time-dependent RANS and VLES : A review, AIAA Journal, **36**, (1998) 173-184.

[7] P.R. Spalart, Detached-eddy simulation, Annual. Review Fluid Mechanics, **41**, (2009) 181-202.

[8] M.L. Shur, P.R. Spalart, M.K, Strelets, A.K. Travin, A hybrid RANS-LES approach with delayed-DES and wall-modelled LES capabilities, "International Journal of Heat and Fluid Flow, **29**, (2008), 1638-1649.

[9] R. Schiestel, A. Dejoan, Towards a new partially integrated transport model for coarse grid and unsteady turbulent flow simulations, Theoretical and Computational Fluid Dynamics, **18**, (2005) 443-468.

[10] B. Chaouat, R. Schiestel, A new partially integrated transport model for subgrid-scale stresses and dissipation rate for turbulent developing flows, Physics of Fluids, **17**, 065106, (2005) 1-19.

[11] B. Chaouat, R. Schiestel, Analytical insights into the partially integrated transport modeling method for hybrid Reynolds averaged Navier-Stokes equations-large eddy simulations of turbulent flows, Physics of Fluids, **24**, 085106, (2012) 1-34.

[12] S.S. Girimaji, Partially-averaged Navier-Stokes method for turbulence : A Reynolds -averaged Navier-Stokes to direct numerical simulation bridging method, Journal of Applied Mechanics, ASME, **73**, (2006) 413-421.

[13] S.S. Girimaji, E. Jeong, R. Srinivasan, Partially averaged Navier-Stokes method for turbulence : Fixed point analysis and comparisons with unsteady partially averaged Navier-Stokes, Journal of Applied Mechanics, ASME, **73**, (2006) 422-429.

[14] F.R. Menter, Y. Egorov, The scale-adaptive simulation method for unsteady turbulent flow prediction : Part 1 : Theory and model description, Flow, Turbulence and Combustion, **85**, (2010) 113-138.

[15] Y. Egorov, F.T. Menter, R. Lechner, D. Cokljat, The scale-adaptive simulation method for unsteady turbulent flow prediction : Part 2 : Application to complex flows, Flow, Turbulence and Combustion, **85**, (2010) 139-165.

[16] B. Chaouat, Subfilter-scale transport model for hybrid RANS/LES simulations applied to a complex bounded flow, Journal of Turbulence, **11**, (2010) 1-30.

[17] B. Chaouat, R., Schiestel, Hybrid RANS-LES simulations of the turbulent flow over periodic hills at high Reynolds number using the PITM method, Computers and Fluids **84**, (2013) 279-300.

[18] I. Befeno, R. Schiestel, Non-equilibrium mixing of turbulence scales using a continuous hybrid RANS/LES approach : Application to the shearless mixing layer, Flow, Turbulence and Combustion, **78**, (2007) 129-151.

[19] B. Chaouat, Application of the PITM method using inlet synthetic turbulence generation for the simulation of the turbulent flow in a small axisymmetric contraction, Flow, Turbulence and Combustion, DOI 10.1007/s10494-016-9794-6, (2017) 1-38.

[20] D. Jeandel, J.F. Brison, J. Mathieu, Modeling methods in physical and spectral space, Physics of Fluids, **21**, (1978) 169-182.

[21] C. Cambon, D. Jeandel, J. Mathieu, Spectral modelling of homogeneous non-isotropic turbulence, Journal of Fluid Mechanics, **104**, (1981) 247-262.

[22] R. Schiestel, Multiple-time scale modeling of turbulent flows in one point closures, Physics of Fluids, **30**, (1987) 722-731.

[23] B. Chaouat, R. Schiestel, From single-scale turbulence models to multiple-scale and subgrid-scale models by Fourier transform, Theoretical and Computational Fluid Dynamics, **21**, (2007) 201-229.

[24] B. Chaouat, R. Schiestel, Partially integrated transport modeling method for turbulence simulation with variable filters, Physics of Fluids, **25**, 125102, (2013) 1-39.

[25] B. Chaouat, R. Schiestel, Progress in subgrid-scale transport modelling for continuous hybrid non-zonal RANS/LES simulations, International Journal of Heat and Fluid Flow, **30**, (2009) 602-616.

[26] M.J. Lee, W.C. Reynolds, Numerical experiments on the structure of homogeneous turbulence, NASA Tech. Memo NCC-2-15, Report No. TF-24. Edited by Stanford University, California, 1985.

[27] R. Schiestel, On the modelling of turbulent flows out of spectral equilibrium, C.R. Académie des Sciences Paris, **302**, 11, (1986) 727-730.

[28] M.S. Uberoi, S. Wallis, Small axisymmetric contraction of grid turbulence, Journal of Fluid Mechanics, **24**, (1966) 539-543.

[29] S. Veeravalli, Z. Warhaft, The shearless turbulent mixing layer, Journal of Fluid Mechanics, **207**, (1989) 191-229.

[30] B. Chaouat, Simulation of turbulent rotating flows using a subfilter scale stress model derived from the partially integrated transport modeling method, Physics of Fluids, **24**, 045108, (2012) 1-35.

[31] J.P. Johnston, R.M. Halleen, D.K. Lezius, Effects of spanwise rotation on the structure of two-dimensional fully developed turbulent channel flow, Journal of Fluid Mechanics, **56**, (1972) 533-557.

[32] E. Lamballais, O. Métais, M. Lesieur, Spectral-dynamic model for large-eddy simulations of turbulent rotating flow, Theoretical and Computational Fluid Dynamics, **12**, (1998) 149-179.

[33] C. Rapp, M. Manhart, Flow over periodic hills - an experimental study, Experiments in Fluids, **51**, (2011) 247-269.

[34] Y. Dubief, F. Delcayre, On coherent-vortex identification in turbulence, Journal of Turbulence, **1**, (2000) 1-22.

[35] L. Shao, J.P. Bertoglio, M. Michard, Large eddy simulation of the interaction between two distinct turbulent velocity scales, Advances in Turbulence, **3**, (1991) 101-112.

[36] S.C. Kassinos, W.C. Reynolds, M.M. Rogers, One-point turbulence structure tensors, J. Fluid Mech., **428**, (2001) 213-248.

[37] V. Mons, C. Cambon, P. Sagaut, A spectral model for homogeneous shear-driven anisotropic turbulence in terms of spherically averaged descriptors, J. Fluid Mech., **788**, (2016) 147-182.

[38] C. Cambon, Etude spectrale d'un champ turbulent incompressible soumis à des effets couplés de déformation et de rotation imposés extérieurement, Thesis Doct. Es. Sc. Phys., Lyon I -Univ. (1982) 213-248.

[39] C. Cambon, L. Jacquin, J. L. Lubrano, Towards a new Reynolds stress model for rotating turbulent flows, Phys. of Fluids A, **4-4**, (1992) 812-824.